more than two-thirds of all grains, 54 out of 75. The group of grains close to Fe = 0, Mg = 50, Si = 50 indicates the survival of primary Mg-rich silicates, which in turn may be taken as evidence for a 'low-temperature' history of the grains, and hence for the primitive nature of Halley's solid dust.

It has been argued from meteor spectroscopy[34] that some of the particles may consist of refractory minerals which resemble Ca, Al-rich inclusions found in certain carbonaceous chondrites and are believed to retain records from the earliest solar system. In the data set analysed in this study, only a few grains with a possibly high Ca + Al content were encountered, but in terms of spectral quality they belong to type 3 and consequently should not be ascribed too great a significance.

Presently the spectra transmitted in the higher compressed modes from the PUMA 1 and 2 and PIA experiments are being evaluated in greater detail; we intend to characterize these spectra by comparing them with the mode-0 PUMA-1 spectra of the present study and also to apply cluster analytical techniques.

We thank Eva Gensel for artwork. Criticism and advice from J. Bradley, E. Grün, E. Anders, D. E. Brownlee and F. R. Krueger are gratefully acknowledged.

Received 28 October 1987; accepted 3 February 1988.

1. Kissel, J. *Eur. Spa. Ag. Spec. Pub.* **1077** 67–68 (1986).
2. Kissel, J. *et al. Nature* **321,** 280–282 (1986).
3. Kissel, J. *et al. Nature* **321,** 336–338 (1986).
4. Jessberger, E. K., Kissel, J., Fechtig, H. & Krueger, F. R. *Eur. Spa. Ag. Spec. Pub.* **249,** 27–30 (1986).
5. Wäsch, R. *Eur. Spa. Ag. Spec. Pub.* **250,** 265–267 (1986).
6. Langevin, Y., Kissel, J., Bertaux, J.-L. & Chassefiere E. *Lunar Planet. Sci. Conf.* **18,** 533–534 (1987).
7. Jessberger, E. K. & Kissel, J. *Lunar planet. Sci. Conf.* **18,** 466–467 (1987).
8. Jessberger, E. K., Kissel, J., Fechtig, H. & Kreuger, F. R. in *Physical Processes in Comets, Stars and Active Galaxies* (ed. Hillebrandt, W., Meyer-Hofmeister, E. & Thomas, H. C.) 26–33 (Springer, Heidelberg, 1987).
9. Sagdeev, R. Z. *et al. Eur. Spa. Ag. Spec. Pub.* **250,** 349–352 (1986).
10. Clark, B., Mason, L. W. & Kissel, J. *Eur. Spa Ag. Spec. Pub.* **250,** 353–358 (1986).
11. Brownlee, D. E., Wheelock, M. M., Temple, S., Bradley, J. P. & Kisssel, J. *Lunar planet. Sci. Conf.* **18,** 133–134 (1987).
12. Mukhin, L. M. *et al. Lunar planet. Sci. Conf.* **18,** 674–675 (1987).
13. Solc, M., Vanysek, V. & Kisssel, J. *Eur. Spa. Ag. Spec. Pub.* **250,** 373–376 (1986).
14. Kissel, J. & Krueger, F. R. *Nature* **326,** 755–760 (1987).
15. Solc, M., Jessberger, E. K., Hsiung, P. & Kissel, J. *Proc. 10th Regional Meeting of the IAU, Prague* (in the press).
16. Jessberger, E. K., Rahe, J. & Kissel, J. in *Origin and Evolution of Planetary and Satellite Atmospheres* (ed. Matthews, M. S.) (University of Arizona Press, in the press).
17. Kissel J. & Krueger, F. R. *Appl. Phys.* **A,** 69–85 (1987).
18. Krueger, F. R. & Kissel, J. *Naturwissenschaften* **74,** 312–316 (1987).
19. Anders, E. & Ebihara, M. *Geochim. cosmochim. Acta* **46,** 2363–2380 (1982).
20. Mason, B. in *Handbook of Elemental Abundances in Meteorites* (ed. Mason, B.) 209–213 (Gordon & Breach, New York, 1971).
21. Anders, E. *Space Sci. Rev.* **3,** 583–714 (1964).
22. Fraundorf, P. *Geochim. cosmochim. Acta* **45,** 915–944 (1981).
23. Wallenwein, R., Blank, H., Jessberger, E. K. & Traxel, K. *Analytica chim. Acta* **195,** 317–322 (1987).
24. SAS Institute Inc. SAS User's Guide: Statistics, Version 5, ed. (Cary, NC: SAS Institute Inc., 1985) 956 pp.
25. Anders, E. *Eur. Spa. Ag. Spec. Pub.* **249,** 31–40 (1986).
26. Hanner, M. *Icarus* **47,** 342–350 (1981).
27. Lewis, R. S., Ming, T., Wacker, J. F., Anders, E. & Steel, E. *Nature* **326,** 160–162 (1987).
28. Irvine, W. M., Schloerb, F. P., Hjalmarson, A. & Herbst, E. in *Protostars and Planets II* (eds Black, D. C. & Matthews, M. S.) 579–620 (University of Arizona Press, Tucson, 1985).
29. Allamandola, L. J., Sandford, S. A. & Wopenka, B. *Science* **237,** 56–59 (1987).
30. Huebner, W. F. *Science* **237,** 628–630 (1987).
31. Bradley, J. P. *Geochim. cosmochim. Acta* (submitted).
32. McKeegan, K. D., Swan, P., Walker, R. M., Wopenka, B. & Zinner, E. *Lunar planet. Sci. Conf.* **18,** 627–628 (1987).
33. Wheelock, M. M. & Brownlee, D. E. *Elemental Composition of Submicron Volumes of Meteoritic Material: Analogs to Cometary Dust Grains* (The Dept. of Astronomy, Univ. of Washington, Seattle, 1986) No. MW9/85.
34. Wilkening, L. L. *Nature* **258,** 689–690 (1985).

Large-scale mantle convection and the aggregation and dispersal of supercontinents

Michael Gurnis

Seismological Laboratory, California Institute of Technology, Pasadena, California 91125, USA

The first time-dependent numerical simulations of continental aggregation and dispersal demonstrate a dynamic feedback between the motion of continental plates and mantle convection. Plate velocity is intrinsically episodic. Continental plates aggregate over cold downwellings and inhibit subduction and mantle cooling; the mantle overheats and fragments the continent under tension. Overall, the models are in agreement with the present geophysical state of the mantle and the geological record over the last 200 million years.

THE breakup of Pangaea which started 180 Myr ago is the dominant event of the late Phanerozoic. Before this breakup, Gondwana and the two northern continents (North America and Eurasia) had assembled together to form the Pangaean supercontinent[1]. Although the evidence is not clear cut, geologists are piecing together a picture of continents aggregating and dispersing a number of times over the last 3,000 Myr (ref. 2 and P. F. Hoffman and S. A. Bowring, unpublished manuscript). How does such aggregation and dispersal take place? It is almost certain that continental motions are tied to a large-scale mode of thermal convection. A physical model of continental aggregation and dispersal has been proposed by Anderson[3] from continental reconstructions, the geoid and from hotspot locations. The supercontinent 200 Myr ago was approximately centred over the Atlantic-African geoid high, but North and South America, Australia, Antarctica and India moved away after breakup. Because this geoid high contains most of the world's hot spots[3–5] and is characterized by low seismic velocities in the lower mantle, it is probably hotter than average[6,7]. The continents (except for Africa) now appear to be moving towards geoid lows, a low incidence of hotpsots, and over lower mantle of high seismic velocity, factors which all indicate cold mantle. These observations suggest that supercontinents could affect the thermal state of the underlying mantle. The mantle underlying the continent becomes hotter than normal, expands and gives rise to geoid highs. This is followed by rifting in the supercontient and the formation of hotspots; the supercontinent fragments and disperses[3].

The feedback between continental plate and mantle convection is fundamental to this model: continental plates insulate the mantle, leading to high mantle temperatures; the perturbed mantle in turn causes continental motions. This two-way interaction has not been investigated in the few model studies of plates and convection. In general, modelling studies can be categorized as either imposing plate characteristics on the top of a convecting region and calculating the effects on convection[8,9] or solving for convection in a region and calculating its effects on the motion of a plate[10,11].

The first dynamically self-consistent numerical models meant to simulate continental plates are presented here; they allow for

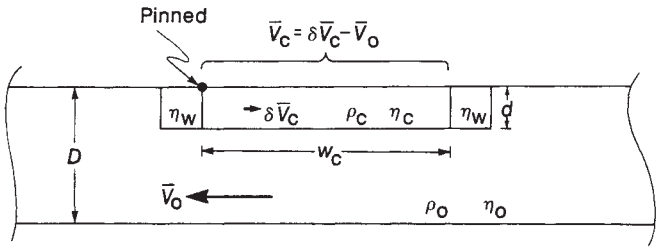

Fig. 1 Schematic of the continental plate within the interior of the convecting fluid. D is the depth of the convecting region. The continent is of viscosity η_c, density ρ_c, width w_c and depth d; other parameters are defined in the text. For the calculations presented here, $\eta_c/\eta_0 = 10^3$, $\eta_w/\eta_0 = 10^{-1}$, and $d/D = 0.125$. The width was a free parameter. Because there were 32 equally sized finite elements in depth, the continent was 4 elements thick. The density difference, $\rho_0 - \rho_c$, was proportional to 20% of the density difference associated with the change in temperature across the box, that is $\rho_0 - \rho_c = 0.2\,\rho_0\alpha\Delta T$, where α is the coefficient of thermal expansion and ΔT the total vertical change in temperature.

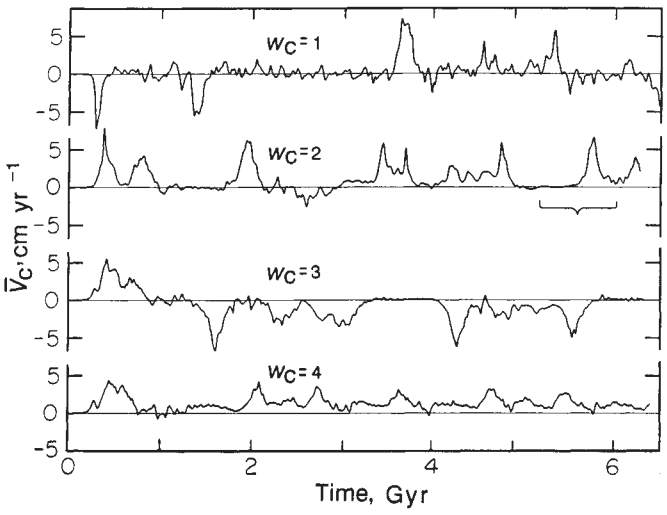

Fig. 2 Continental plate velocity $\bar{V}_c$, versus scaled model time, for four plate widths, w_c. The scaling parameters are given in Fig. 4. Each model was run for 14,000 'Courant' time steps.

a two-way interaction between internal convection and unsteady plate motion. The case of a single plate floating on top of the convecting region is studied, and the analysis is extended to two plates that can heal into a single plate, such as a supercontinent, and subsequently break up into two independent continents. The results for a single plate show that convection velocity is intrinsically episodic so that the continental plate experiences short bursts of rapid velocity. When a 'breakable' long plate is introduced, it will remain stationary, and the underlying fluid will heat up and break the plate into two fragments that rapidly move away from the hot area. The periodicity of this behaviour is ~100–1,000 Myr, the variation in horizontal compressive and tensile stresses are ~10–10^2 MPa, peak plate velocities are ~5 cm yr^{-1}, and the subcontinental lithosphere temperature varies over a few hundred degrees Celsius. This insulation-induced heating mechanism, which gives rise to large-scale horizontal temperature variations, is in strong agreement with the geological record.

Model parameters

Thermal convection is calculated using the finite element method in a two-dimensional long box; the fluid is incompressible, has an infinite Prandtl number and a Rayleigh number of 10^5. The code, which solves for the temperature equation explicitly and the Stokes equation with a penalty function formulation, has been extensively compared with other codes[12]. The box has an aspect ratio (length/depth) of eight, and periodic boundary conditions; this means that fluid can flow out of one side of the box and into the other. For simplicity, the temperatures on both the base and top are held constant, a constant background viscosity is used and there is no internal heating in the fluid or plates. Without plates, this gives rise to Rayleigh-Bénard convection, the best understood mode of thermal convection treated by solid-Earth geophysicists[13].

A continental plate is introduced by assigning high viscosity and an intrinsic chemical buoyancy to a group of elements along the top. The thermal properties are constant throughout the whole system. As illustrated in Fig. 1, the following variables are defined: the non-dimensional width and depth of the continental plate (w_c/D and d/D) and the density and viscosity of the continent (ρ_c/ρ_0 and η_c/η_0). The two sides of the continent are bounded by zones of low viscosity, η_w/η_0. The top and bottom surfaces have free-slip boundary conditions, except for one pinned node that defines one corner of the continental plate. The average horizontal velocity through the box, excluding the continent, is $\bar{V}_0$, and is an ouput parameter of the calculation. If the continent had zero velocity, then the continental velocity with respect to the fluid would be $-\bar{V}_0$; this would be the case if all of the nodes in the continent were pinned or if $\eta_c/\eta_0 \to \infty$. Because neither case is true, however, there are small velocity variations throughout the plate and consequently there is a residual velocity, $\delta\bar{V}_c$. The continental velocity is thus $\bar{V}_c = \delta\bar{V}_c - \bar{V}_0$. This may appear to be overly complex, but if there are several continents then only one can be pinned and the other(s) must move with respect to the pinned node, which is the second problem to be studied here. It turns out that for $\eta_c/\eta_0 = 10^3$, $\delta\bar{V}_c/\bar{V}_0 < 10^{-3}$. This formulation, with the continent pinned, allows a great reduction in the computation time. The stiffness matrix in the finite element formulation always remains the same and it need be formed and inverted only at the start of the time-dependent problem.

The case of two continents requires a few changes from the one-plate case. One plate is formed, as previously, with one node pinned, but the second plate must be advected. The average horizontal velocity is calculated in the second plate and the 'stencil' defining which elements have η_c and ρ_c is advected with this velocity. As the viscosities of the elements change during the model run, the stiffness matrix must be reformed and inverted; this reforming becomes more frequent when two plates are moving rapidly with respect to each other, and does not occur when the plates are joined together. Criteria must be defined for breaking one long plate into two short ones and vice versa. First, the areal average of the stress, σ_{xx}, is calculated from the velocity field. A plate is broken when σ_{xx} exceeds a critical yield stress, σ_{yld}, in which case each edge of the single plate moves slightly outwards and the centre high viscosity, η_c, is replaced by low viscosity, η_w. For simplicity, the low-viscosity zones are retained on the edges of the plate. When two plates are converging and the two low-viscosity zones overlap, the low viscosity, η_w, is replaced by η_c and the plate heals.

The intention of this model problem is not to simulate the entire plate tectonic-mantle convection system. Rather, the intention is to study one important feedback mechanism between plates and convection. Consequently, some aspects have been simplified from the true Earth, in particular the fact that in the oceanic areas there are no stiff plates. This is not a great drawback, however, because the oceanic areas still retain the fundamental property of having convection extending directly to the surface (oceanic lithosphere) and having the fluid that is cooled on the surface returned to the interior (subduction). The distinction between continents and oceans in this case is a 'conducting lid' on part of the fluid and free convection on the other part. Unique to this study is that the 'conducting lid' (continental

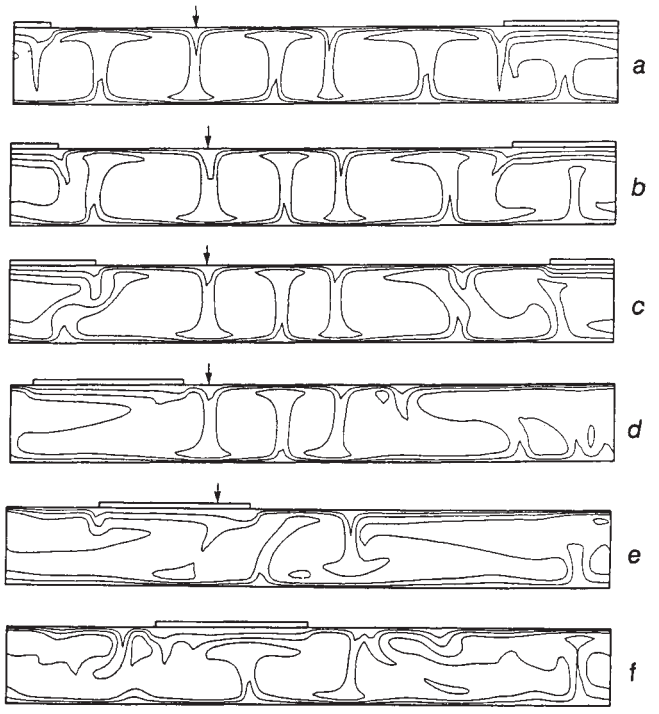

Fig. 3 Isotherms at four instants in a simulation involving a single plate of width, $w_c = 2$. The narrow box on the top of the fluid denotes the location of the plate; the height of the box has no physical significance as the continental plates are actually within the fluid. The vertical arrows denote a cold downwelling towards which the continental fragment moves. The Rayleigh number for the calculations was 10^5. This figure was formed by computing a reference offset which was integrated forward with $\bar{V}_c$. This offset was then added to the raw temperature field and plate position.

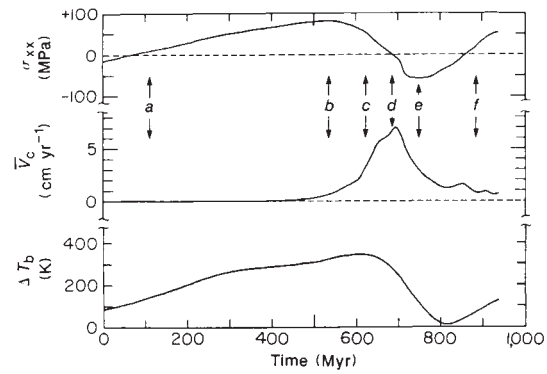

Fig. 4 Average horizontal stress through the plate, σ_{xx}, plate velocity, $\bar{V}_c$, and the change in temperature beneath the plate ΔT_b, for a single plate of width $w_c = 2$, as shown in Fig. 3. The letters labelling instants in time correspond to the isotherm plots in Fig. 3. The following parameters were used to scale the non-dimensional model results: a mantle depth of 3,000 km, an average mantle density of 4,000 kg m^{-3}, an average viscosity for the whole mantle of 5×10^{21} Pa s, a total mantle temperature drop of 2,800K, a coefficient of thermal expansion of 2×10^{-5} K, and a thermal diffusivity of 10^{-6} m^2 s^{-1}. Parameters from ref. 23. These parameters give a Rayleigh number of 6×10^7. Preliminary Rayleigh number scalings were determined by obtaining $\bar{V}_c$, σ_{xx} and T_b at $10^4 \leq Ra \leq 10^{5.5}$: $\bar{V}_c$ and σ_{xx} were written 10 per cent of the values obtained through boundary layer scalings[23]; T_b has a complex functional form, but is approximately independent of Ra at $Ra > 10^5$. For the scalings, the boundary layer equations[23] were used for $\bar{V}_c$ and σ_{xx} and T_b is assumed independent of Ra. The non-dimensional values were then scaled using the above mantle parameters; the final scaled $\bar{V}_c$, σ_{xx} and T_b are only accurate to within a factor of two.

plate) can go anywhere and take any velocity it chooses, allowing us to study some important feedback mechanisms that may cause continental drift. The next generation of these dynamic simulations will require both oceanic and continental plates, perhaps generated by a stress- and temperature-dependent rheology.

Single plate

Much of the physics experienced by breaking and healing plates will be contained in the motion of a single plate; for this reason single plates will be considered in detail here and the breaking-healing plates are presented as an extension to the present analysis. Through the rest of this article, the non-dimensional results are scaled to the Earth. This involves both scaling to a higher Rayleigh number as well as dimensionalizing using appropriate mantle values (see legend to Fig. 4); considering both aspects of the scalings, the final values (for example, the plate velocity, stress and basal temperature) are uncertain and are only accurate to within a factor of two. In Fig. 2 the velocity, $\bar{V}_c$, of single plates is presented for four widths, w_c, between 1 and 4. As seen in Fig. 2, plate velocity is not constant in any of the four cases; instead the velocity is distinctly episodic. For $w_c \leq 2$, periods of zero or low velocity are interrupted by short bursts of high velocity.

The cause of this velocity episodicity can be understood by carefully tracing the thermal and stress history of the fluid and plate through one cycle of the velocity pattern. Isotherms are shown in Fig. 3 and plate stress, velocity and temperature in Fig. 4 for $w_c = 2$. Starting with Fig. 3*a*, the continental plate is trapped between two cold downwellings, and directly over an upwelling. The plate is stationary and has zero average horizontal stress, σ_{xx} (Fig. 4*a*). The average temperature along the base of the plate increases linearly by about 1 °C every 2.5 Myr for ~450 Myr (Fig. 4*b*), while the plate remains stationary. As indicated in Fig. 3*b*, the cold downwellings on the sides of the plate are pushed aside as the sub-plate mantle becomes heated. In this heated state the plate is under significant tension (~70 MPa). The cold downwellings can no longer keep the plate trapped and it rapidly moves off the hot upwelling, relaxing the high tensional stress. A peak velocity of ~7 cm yr^{-1} is reached (Fig. 3*d*) at about the same time that σ_{xx} is reduced to zero; the sub-plate temperature also peaks ($\Delta T_b \sim 250$ °C) just before maximum plate velocity is achieved. In Fig. 3, a vertical arrow indicates the closest downwelling off to the right of the original plate position; Fig. 3*b*-*e* shows the plate moving toward this downwelling and coming to rest over it. As the plate settles over the downwelling, the stress moves into a compressive state (Fig. 3*e*) of more than 50 MPa. The gross topography of the plate can be estimated from the average horizontal vertical stress. Initially, the plate is topographically high and reaches a peak elevation when σ_{xx} is at a maximum (Fig. 3*b*), but rapidly subsides during rapid plate motion; the total (peak to peak) variation in topography over time is ~3 km. The part of the fluid vacated by the plate is significantly overheated with a thin thermal boundary layer on the top surface (Fig. 3*d*). This is an unstable state and the convecting fluid passes into a chaotic flow regime (Fig. 3*f*). Although this is a subject of active research[14], benchmarks at different resolutions suggest that this chaos is adequately resolved with the 33 nodes in depth[12]. The cycle starts in an organized state with regularly spaced convection cells (Fig. 3*a*) but ends in a disorganized state (Fig. 3*f*), although in both instances the average plate velocity is either zero or very low.

The cycle just described is general, but the period and relative length of the stationary interval to rapid-velocity interval is dependent on plate size: the period between bursts of high velocity decreases with increasing plate width, until by $w_c \approx 4$ the plate always has an appreciable velocity (Fig. 2). Apparently, for this relatively long plate, a large-scale horizontal temperature gradient always exists and continually pushes the plate along, although there are still short bursts of higher velocity. For

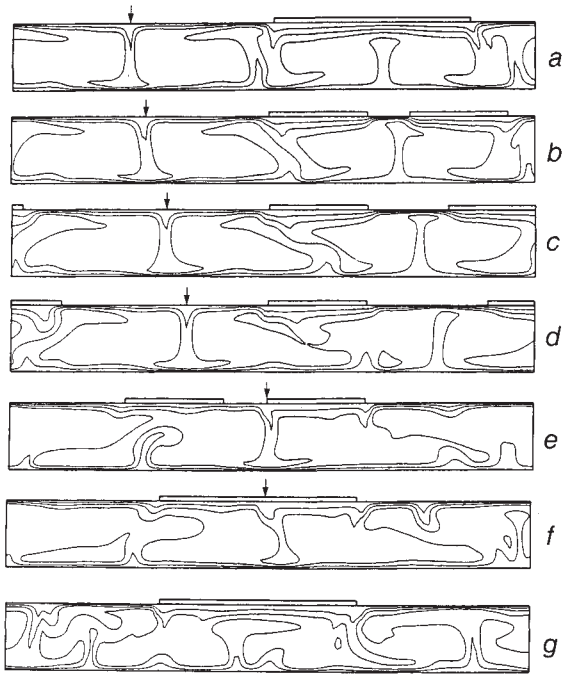

Fig. 5 Isotherms for a plate of $w_c = 3$ which breaks into two plates of $w_c = 1.5$ under a tensile yield stress, σ_{yld}, of 70 MPa. The arrow points toward a cold downwelling which the continental fragments move toward after break-up. The frame of reference is fixed with respect to the left corner of the original plate; the right plate in frame *b* moves with respect to the left plate, which is stationary in this reference frame.

$1 \leq w_c \leq 3$ the peak continental plate velocity is almost constant at ~7–8 cm yr^{-1}, whereas for $w_c = 4$, the peak velocity is distinctly less, ~4.5 cm yr^{-1}. The root mean square of the velocity histories of Fig. 2, however, are almost constant for all cases, including $x_c = 4$, at ~1.5–2.0 cm yr^{-1}, with some suggestion of a peak between $w_c = 2$ and 3. For small widths, $w_c \ll 1$, the plate has no effect on the flow and aligns itself perfectly on top of a downwelling; if the flow is intrinsically steady, which is true for the Rayleigh number used in this study, then the plate velocity will be zero.

Breaking–healing plate

We now extend our analysis to the case of a long plate that can break under tension and heal upon collision; this model problem may contain most of the relevant physics involved in the breakup and assembly of supercontinents. As the starting state for the breaking-healing plate, an instant from a single plate run with $w_c = 3$ was used. When the plate breaks, each plate of the pair will have $w_c = 1.5$. The tensile yield stress, σ_{yld}, was set at 70 MPa, a reasonable value based on the failure of rocks studied in the laboratory[15]. Figure 5*a* is a few time steps before σ_{xx} reached σ_{yld}. If this plate could not yield under tension then the subplate temperature would have increased further, making σ_{xx} >70 MPa. In Fig. 5*a*, the plate is in a stable state with cold downwellings on either side and a hot upwelling in the centre. If more freedom were allowed in the break-up algorithm, the plate would still break in the centre because of symmetry. The frame of reference for Fig. 5 is with respect to the left margin of the original plate, such that the fluid in the box will flow by this stationary plate; this frame of reference is different from that of Fig. 3 which was in the mantle frame.

Immediately after the long plate breaks, the two smaller pieces start separating rapidly with a velocity of ~7 cm yr^{-1} by 4 Myr. By 18 Myr after break-up (Fig. 5*b*), the plates are separating at 10.5 cm yr^{-1}. Moreover, the hot upwelling extends to the surface between the two continental plates and forms a thin thermal boundary layer. The cold downwellings, originally on the two edges of the long plate, now point toward the region of hot upwelling (Fig. 5*c*). Both plates rapidly move toward the cold downwellings on the other side of the box (marked with an arrow, Fig. 5). As the frame of reference is with respect to the left corner of the orginal long plate (now the centre plate), this cold downwelling is seen to move toward the centre plate. The two plates collide ~150 Myr after breakup. As in the case with the single plate, the area vacated by the continental plates is significantly overheated and undergoes frequent boundary layer instabilities which bring the fluid into a chaotic flow regime. After break-up, the two small plates spend most of the time under compressive horizontal stress. Immediately after assembly, the new long plate is under compression and positioned over the cold and downward flowing part of the fluid (Fig. 5*f*). In Fig. 5*g*, nearly 450 Myr after break-up, a new upwelling has developed under the plate. An estimate of the overall topography variation of the plate can be deduced from σ_{zz}. The peak-to-peak variation in topography is ~3.5 km from a high elevation before and during break-up to a minimum elevation following assembly.

A slightly different model has been run for a significantly longer period of time; in Fig. 6 the horizontal axis is distance across the top of the convecting fluid, and the vertical axis is time. Continental plates are denoted in black. This model differs from the case in Fig. 5 in that a smaller yield stress is used ($\sigma_{yld} = 50$ MPa) but the aggregated plate has the same width ($w_c = 3$). The run starts with the plate in the aggregated state and remains that way as it undergoes slow lateral translation at ~1 cm yr^{-1}; the plate breaks at 700 Myr. The fragments move apart and assemble again after 350 Myr, having reached velocites of up to 7 cm yr^{-1}. At the 700 Myr break-up, the flow exhibited a significant degree of order with only one major downwelling opposite the supercontinent, so that reassembly was relatively rapid; this is similar to the case shown in Fig. 5 which had a higher yield stress. At 1,100 Myr the reassembled continent remains stationary and insulates the mantle, so that after about another 400 Myr the continent breaks up again. After the 1,500-Myr break-up, the flow is quite chaotic and each continental fragment comes to rest over a different cold downwelling (at 1,900 Myr); the chaos apparently inhibits the fragments from reassembly for at least the next 2,000 Myr. Clearly, break-up is an almost certain occurrence if a supercontinent is assembled but assembly of small fragments over the same cold downwelling can be a long term process controlled by the number of downwellings and the degree of chaos in the flow. During the 3,500 Myr-model run, two break-ups and one assembly occurred. The continents were disassembled or fragmented for 70% of the time.

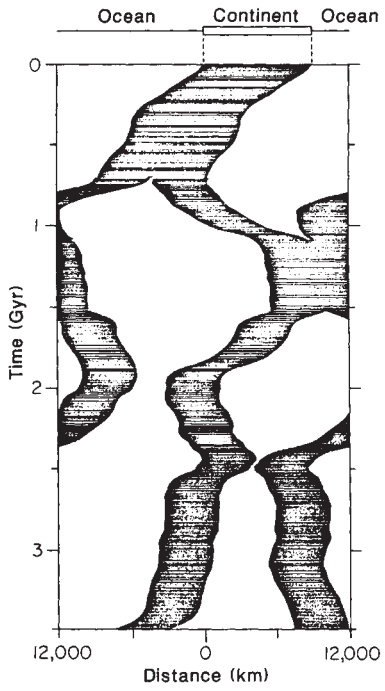

Fig. 6 Geometry of the continental plate as a function of time. The continental plates are denoted in black. The parameters used to scale the results are given in Fig. 4 legend.

Discussion

Despite the apparent simplicity of the models, the physics just outlined is in overall agreement with the geological record, especially during the last 200 Myr since the breakup of Pangaea. The Pangaean supercontinent, in its completely assembled state, was positioned over what is now the Atlantic-African geoid high[3]. Unfortunately we have no direct evidence of the form of the geoid 200 Myr ago, but today the Atlantic-African geoid high (like the Pacific geoid high) is strongly correlated with the location of present-day hot spots[3-5]. If the geoid high was correlated with hotspots 200 Myr ago, then it must have been approximately centred over Africa, as Africa has moved only slowly with respect to hotspots since breakup. The geoid high and hotspots are also correlated with slow seismic velocities in the lower mantle at spherical harmonic degree two, where most of the power is for both the geoid and the hot-spot locations[6,7]. These observations are consistent with a lower mantle that was hotter than average under Pangaea before break-up, exactly as predicted by the numerical models. Since the supercontinent break-up, the continental fragments North and South America, Antarctica, Australia and India have been moving towards geoid lows[16].

The present-day pattern of stress in continents is also consistent with the state of stress in the modelled plates. The models predict that after break-up, when continental plates are settling in over cold downwellings, plates should be in a compressive state. In general most continental plates are in a state of compression[17-19]; the exception is Africa, which has significant portions under tension[17]. This anomalous pattern for Africa is consistent with its lying over hot mantle, as indicated by the geoid, hotspot locations and lower-mantle seismic tomography. Following the break-up of Pangaea, the continents experienced major transgressions in the late Cretaceous[20], a transgression being consistent with continental subsidence, a rise in sea level, or a combination of both[20]. The numerical models predict a rapid rise in relative sea level or relative subsidence after continental break-up.

Within uncertainty, the time scales and plate velocity are also consistent with observations. Just after the Pangaean break-up, the average continental velocity was ~ 4 cm yr^{-1} (ref. 21) and there has been an apparent slowing down of the continents since then, present day velocity being ~ 2 cm yr^{-1} (refs 21, 22). This is consistent with the continents slowing down over cold-mantle downwellings. This 4-cm yr^{-1} observed velocity is somewhat lower than that of the model presented in Fig. 5 which had a separation velocity of 10 cm yr^{-1}. In general, it took a few hundred Myr for the modelled continents to settle in over cold downwellings after break-up. This reassembly time scale is dependent on both the aspect ratio of the box and the number of cold downwellings in the oceanic area before supercontinent break-up. For the case in Fig. 5, a high degree of order is present with only one cold downwelling opposite the long plate; this situation provided the minimum distance for fragments to traverse and reassemble, and hence a minimum time for the aggregation dispersal cycle. A maximum time required for the plates to move off hot mantle and toward cold downwellings is about 1,000 Myr; this is a maximum time because breaking plates move off sooner with a value determined somewhat by the tensile yield stress. A crude estimate of the time between assembled supercontinents, inferred from the numerical models, is in the range of a few hundred Myr up to two thousand Myr, with preferrred values on the high end. Anderson[3] suggests that the continents were dispering 500-350 Myr ago (the state the continents are in today), so that the observed cycle time may be ~ 500 Myr, consistent with the numerical results.

Discussions and valuable reviews were provided by Don Anderson and Bradford Hager. The work was supported by the NSF and a grant from the Ametek Corporation. Computing was carried out on the facilities of the San Diego Supercomputer Center.

Received 20 November 1987; accepted 7 March 1988.

1. Smith, A. G., Hurley, A. M. & Briden, J. C. *Phanerozoic Palaeocontinental World Maps* (Cambridge University Press, 1981).
2. Kerr, R. A. *Science* **230**, 1364-1367 (1985).
3. Anderson, D. L. *Nature* **297**, 391-393 (1982).
4. Crough, S. T. & Jurdy, D. M. *Earth planet. Sci Lett.* **48**, 15-22 (1980).
5. Chase, C. G. *Nature* **292**, 464-468 (1979).
6. Hager, B. H., Clayton, R. W., Richards, M. A., Comer, R. P. & Dziewonski, A. M. *Nature* **313**, 541-545 (1985).
7. Hager, B. H. & Clayton, R. W. in *Mantle Convection* (ed. Peltier, W. R., in the press).
8. Hager, B. H. & O'Connell, R. J. *J. geophys. Res.* **86**, 4843-4867 (1981).
9. Davies, G. F. *Geophys. J. R. astr. Soc.* **84**, 153-183 (1986).
10. Olson, P. & Corcos, G. M. *Geophys. J. R. astr. Soc.* **62**, 195-219 (1980).
11. Schmeling, H. & Jacoby, W. R. *J. Geophys.* **50**, 89-100 (1981).
12. Hager, B. H. *et al. Los Alamos National Laboratory Technical Report* (in the press).
13. McKenzie, D. P., Roberts, J. M. & Weiss, N. O. *J. Fluid Mech.* **62**, 465-538 (1974).
14. Vincent, A. P. & Yuen, D. A. *University of Minnesota Supercomputer Institute Technical Report* **87/56**.
15. Brace, W. F. & Kohlstedt, D. L. *J. geophys. Res.* **85**, 6248-6252 (1980).
16. Anderson, D. L. *Science* **223**, 347-355 (1984).
17. Richardson, R. M., Soloman, S. C. & Sleep, N. H. *Rev. Geophys. Space Phys.* **17**, 981 (1979).
18. Zoback, M. L. & Zoback, M. *J. geophys. Res.* **85**, 6113-6156 (1980).
19. Lambeck, K., McQueen, H. W. S., Stephenson, R. A. & Denham, D. *Ann. Geophys.* **2** 723-742 (1984).
20. Bond, G. *Geology* **4**, 557-560 (1976).
21. Schult, F. R. & Gordon, R. G. *J. geophys. Res.* **89**, 1789-1800 (1984).
22. Irving, E. *Nature* **270**, 304-309 (1977).
23. Turcotte, D. L. & Schubert, G. *Geodynamics* (Wiley, New York, 1982).